Smoothening of the non-Euclidean surface of Nd_2O_3 doped CeO_2 nanoceramic grains under sintering: an ultra-small angle x-ray scattering investigation and a computer simulation study

2008 J. Phys.: Condens. Matter 20 035103

(http://iopscience.iop.org/0953-8984/20/3/035103)

IOP PUBLISHING JOURNAL OF PHYSICS: CONDENSED MATTER

J. Phys.: Condens. Matter **20** (2008) 035103 (7pp) doi:10.1088/0953-8984/20/03/035103

Smoothening of the non-Euclidean surface of Nd_2O_3 doped CeO_2 nanoceramic grains under sintering: an ultra-small angle x-ray scattering investigation and a computer simulation study

D Sen[1], J Bahadur[1], S Mazumder[1], V Bedekar[2] and A K Tyagi[2]

[1] Solid State Physics Division, Bhabha Atomic Research Centre, Mumbai-400 085, India
[2] Chemistry Division, Bhabha Atomic Research Centre, Mumbai-400 085, India

E-mail: debasis@barc.gov.in (D Sen)

Received 17 August 2007, in final form 14 November 2007
Published 10 December 2007
Online at stacks.iop.org/JPhysCM/20/035103

Abstract

Smoothing of the fractal rough surface of Nd_2O_3 doped CeO_2 ceramic under sintering has been observed in an ultra-small angle x-ray scattering investigation. The surface fractal dimension of 2.6 for the non-sintered specimen reduces with sintering temperature and gradually attains a value of 2.0, which corresponds to a smooth surface, at a high enough sintering temperature. A Monte Carlo based computer simulation has been attempted to explain the smoothing of such a fractally rough surface due to the diffusion based surface transport of the materials from a region of positive curvature to one of negative curvature. The variation of the interface width and the evolution of the fractal dimension with sintering have been estimated from this model simulation.

(Some figures in this article are in colour only in the electronic version)

1. Introduction

In many natural and synthetic objects, the structures manifest in such a way that it asks for the introduction of a new dimension, which is different from its normal Euclidean dimension, for mathematical description and quantification of its structures. Since Benoît Mandelbrot first brought the idea of fractals [1] to the attention of the world, self-similarity/self-affinity has wormed its way into the various branches of sciences as well as in psychology and even abstract arts. Many naturally occurring materials like rocks [2, 3], coals [4, 5], cauliflowers, some special coastlines etc are some examples of such natural fractal objects. Synthesized objects like hydrated cement pastes [6, 7], surfaces prepared by molecular beam epitaxy etc. also are known to be fractal in nature and the fractal nature depends strongly on their synthesis route. An object which is fractal over a wide length scale can be either mass fractal [8] or surface fractal [8] in nature. For a mass fractal object, the mass or the volume is proportional to r^{d_m}, where d_m is known as the mass fractal dimension, which is less than 3. For a surface fractal object, the self-similarity or the self-affinity exists only on the surface of the object. In this case the surface area scales with r^{d_s}, where d_s is known as the surface fractal dimension. The value of d_s is more than 2 but less than 3. It is noteworthy that for a smooth surface the surface area scales with r^2. A mass fractal object, by default, is also a surface fractal, but a surface fractal object need not be a mass fractal object.

Nanocrystalline materials, which have gained tremendous attention in basic sciences as well as in technology in the last decade, often form agglomerates because of their very small size. Often such agglomerates, vis-à-vis the surface roughness of these nanocrystalline materials, can be viewed as self-similar or self-affine fractal structures. The fractal dimension (d_f) defines the quantitative measure of such fractal agglomerates, which is different from the normal Euclidean dimension.

The microstructural evolution of such nanocrystalline ceramics under sintering is a crucial aspect as far as their various potential applications are concerned. Fine powders offer sintering at relatively low temperature. In general, in the sintering process, the densification occurs via the path where the surface energy is reduced by the elimination of the solid–pore interfaces. The reduction of the free energy is effected by the movement of the materials from the region with higher radius of curvature to that with the lower radius of curvature causing densification. The sintering behaviour of the powders, where the basic particles under sintering are free from agglomeration, has been studied extensively in the past and well understood [9]. But for the nanocrystalline powders the agglomerate being soft or hard affects the sintering behaviour. In addition the sintered microstructure depends on the nature of the agglomerates. In many cases, because of the agglomerated nature of the initial powders, the surface of the particles does not remain exactly smooth; a roughness comes into the picture. The surface microstructure and the agglomeration behaviour change with the advancement of the sintering process and mainly depend on the sintering temperature/time.

Small angle x-ray scattering (SAXS) [10, 11] is an indispensable technique for probing such self-similar or self-affine density fluctuations in materials in a statistically averaged way [10, 11] on mesoscopic length scales. It is a speciality of small angle scattering that it can differentiate [12] between the mass fractal and the surface fractal nature. Monte Carlo based computer simulation may be performed to understand the nature of the evolution of the density fluctuations on the surface of a fractal object on the basis of the SAXS results.

Doped ceria is an important material [13, 14] in view of its potential applications [15] as a solid electrolyte for use in oxygen concentration cells and in solid oxide fuel cells. The high ionic conductivity coupled with the low activation energy for ionic conduction makes doped ceria an attractive material for use at temperatures below 800 °C, which would allow greater flexibility in design of electrodes and inter-connectors [13]. Doped ceria is also a potential candidate for controlling the air to fuel ratio in automobile exhausts [16]. Addition of trivalent Nd^{3+} increases the ionic conductivity of ceria.

In the present paper we have investigated, using ultra-small angle x-ray scattering (USAXS) [17], the evolution of the density fluctuations on the mesoscopic length scale in $Ce_{0.50}Nd_{0.50}O_{1.75}$ [14] under sintering. An attempt has been made to understand the USAXS results by performing a Monte Carlo based simulation.

2. Experimental details

2.1. Sample

AR grade cerium nitrate [$Ce(NO_3)_3{\cdot}6H_2O$], Nd_2O_3, and glycine (NH_2CH_2COOH) were used as the starting reagents. The detail of the sample preparation technique through the precursor and auto-ignition route has already been described in an earlier paper [14]. The further heat treatment of the $Ce_{0.50}Nd_{0.50}O_{1.75}$ powder was carried out at three temperatures, namely, 800, 1000 and 1200 °C, successively. For the USAXS experiments the thin layer powder specimens was prepared on a Kapton tape.

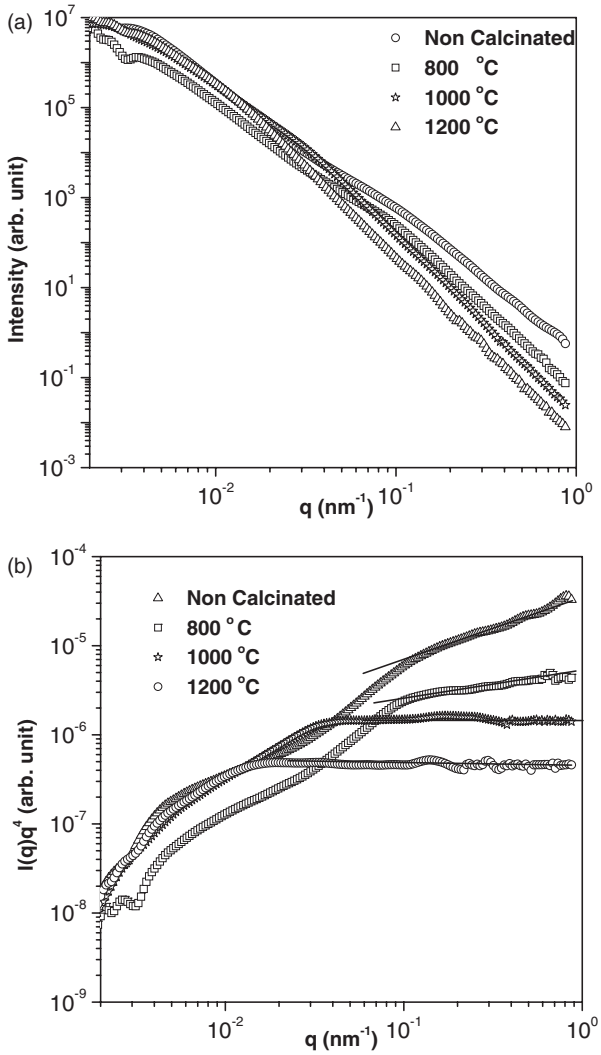

Figure 1. (a) USAXS profiles on a double-logarithmic scale. (b) USAXS profiles in a Porod plot ($I(q)q^4$ versus q). The solid line in the high q region is a guide to the eye to show the change in the Porod slope at high q with sintering temperature.

2.2. USAXS experiment

USAXS experiments were carried out using a triple-bounce channel cut crystal based USAXS instrument mounted on a rotating anode source [18] at the *Laboratoire Interdisciplinaire sur l'Organization Nanométrique et Supramoléculaire* (LIONS), at the CEA, Saclay, France. The instrument consists of a non-dispersive (1, −1) setting of 111 reflections from germanium single crystal with the specimen between the two crystals. The scattered intensities were recorded as a function of the wavevector transfer q [$=4\pi \sin(\theta)/\lambda$, where 2θ is the scattering angle and λ (=0.154 nm) is the incident x-ray wavelength of the Cu Kα radiation]. The measured USAXS profiles have been corrected for background, transmission and instrument resolution effects [19]. Figure 1(a) shows the USAXS

profiles on double-logarithmic scales and figure 1(b) depicts the same profiles in a Porod plot ($I(q)q^4$ versus q) in order to show clearly the variation in slope of the different profiles at higher q.

3. USAXS data analysis

From figure 1(a) it is discernible that the profile for the non-sintered sample shows a straight line behaviour in a log–log plot (i.e., a power law relationship with q). In addition, there is a slight change in slope at around $q \sim 0.1$ nm^{-1} where a small hump appears [20]. From figure 1(b) it is evident that the slope of the profile is not equal to 4 for any part of the q range. The exponent of the power law for $q > 0.1$ nm^{-1} is ∼3.4 for the non-sintered sample. It is also evident from figure 1(a) that the high q part of the profile is significantly affected by sintering, particularly the value of the slope in the higher q region. With increase in temperature of the sintering, the value of the slope at higher q tends to ∼4 and the hump at ∼0.1 nm^{-1} disappears. The above observations, along with that of the nature of the high q region, guide us to analyse the data in terms of the fractal model. It is noteworthy that due to the power law correlation in the fractal systems in real space, the SAXS profile also manifests a power law in q [12, 21]. The exponent of that power law is a non-integer and depends on the nature of the fractal. For a mass fractal object, the SAXS intensity $I(q)$ follows $q^{-\alpha}$ behaviour for the relatively high q region with respect to the inverse of the upper fractal cut-off. In this case the mass fractal dimension (d_m) is equal to the value of α. However, in such a case $\alpha \leqslant 3$. For a surface fractal object $4 \geqslant \alpha \geqslant 3$ and in this case the surface fractal dimension (d_s) is equal to the value of $6-\alpha$ and lies between 2 and 3. For an ideally smooth surface ($d_s = 2.0$), $I(q)$ obeys the Porod law in the high q region, i.e., $I(q)$ follows a q^{-4} behaviour.

For the non-sintered sample, the negative exponent of the power law (for 1 nm$^{-1} > q > 0.1$ nm^{-1}) is estimated to be nearly 3.4. This hints that the surface of the agglomerated particles may be viewed as a fractal surface. Here it is worthy of mention that mathematical fractals like the Sierpinski gasket [22] are exactly self-similar. However, most real fractal objects observed in natural or in synthesized materials are not exactly self-similar but self-affine in nature, which means that these are fractals in some statistical sense and the scaling parameter is not truly isotropic but imposes some directional dependence. As the small angle scattering study gives statistically averaged information, the data from real self-affine objects can be modelled in terms of fractals in order to quantify the structure. It is observed from figure 1(b) that the negative exponent of the power law gradually reaches 4 with sintering at increasing temperatures, indicating a smoothing of the surface roughness of the particles. For the non-sintered samples, the intensity also increases below the hump at around 0.1 nm^{-1}. The total intensity profile $I(q)$ for the samples has been modelled as follows:

$$I(q) = C_s q^{-1}(1+q^2\xi_s^2)^{(\frac{d_s-5}{2})}\sin((d_s-1)\tan^{-1}(q\xi_s)) + \frac{C_a}{(1+q^2\xi_a^2)^n} \quad (1)$$

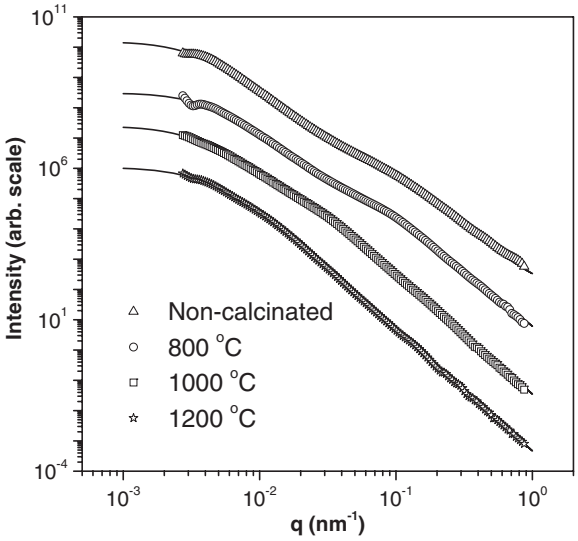

Figure 2. The fit of the model curve to the USAXS data.

Table 1. The parameters obtained from the fit of the model to the USAXS data.

Sample	d_s	ξ_s (nm)	ξ_a (nm)	N	C_a/C_s
Non-sintered	2.60	17	250	2	5.5×10^5
800 °C	2.40	17	250	2	2.9×10^5
1000 °C	2.02	49	250	2	9.0×10^4
1200 °C	2.00	220	—	—	—

where the first term corresponds to the scattering from the fractal surface [23] and the second term is the Debye–Büche term [24, 25] present to account for the increase below the hump. Such an increase is due to the agglomerated volume at relatively large length scale. Shah *et al* [25] have used the Debye–Büche function to interpret their data on dense highly polydisperse fractal aggregates. C_s and C_a are the scale factors and ξ_s is the upper cut-off of the surface fractal nature. The scale factors are q independent but depend on the contrast as well as on the number density of the particles. The parameters estimated from the non-linear least squares fitting of the model to the data are tabulated in table 1. The fit of the model to the data is shown in figure 2. For the sample sintered at the highest temperature (1200 °C), the first term alone is able to describe the whole profile (which follows a Porod behaviour (q^{-4}) at high q) and in this case the surface becomes smooth in nature, i.e., d_s becomes 2.

It is obvious from the table that the value of the surface fractal dimension (d_s) gradually tends to 2 with increase in sintering temperature and the final result is a smooth surface, starting from a fractally rough surface.

4. Monte Carlo based computer simulation and discussions

The Monte Carlo method provides a platform for simulating various stochastic processes in materials science. The area of fractals has also been enriched, in the last two decades, by applying this technique. The self-similarity and fractal nature

of a roughening interface has been studied using the two-dimensional Monte Carlo technique [26] by Mon *et al*. Scaling of rough surfaces under surface diffusion has been investigated using a random deposition model in two dimensions [27]. Monte Carlo simulation has also been applied to predict a high fractal dimension and surface roughening for sedimentary rocks [28, 29]. Very recently a stochastic simulation model has been applied to model the three-dimensional morphology of nanoscaled aggregates formed by concurrent coagulation and sintering [30].

In the present paper, to understand the USAXS results, i.e., the smoothing of the fractal surface under sintering, a Monte Carlo based simulation has been attempted. The basic steps of the simulations are the following.

(a) Initially, a self-affine fractal surface with a particular surface fractal dimension is generated using a Fourier filtering based spectral synthesis method [31].
(b) Once the fractal surface is generated, the effect of sintering under different temperature conditions is studied by modifying the surface according to the movement of materials via a diffusion mechanism.

The algorithm followed in the present case is as follows.

Let $h(x, y)$ define the height of any randomly chosen point $P(x, y)$ on the fractal surface. First it is checked whether the point P has a positive curvature. Then another point $P'(x', y')$ on the surface is chosen randomly. If the point $P1$ (at height $(h'(x', y')$) has a negative curvature, then the curvature difference $\Delta\gamma$ (i.e., the difference between the height of P and the average height of all the nearest neighbours) and the height difference Δh are calculated. If the activation energy is ΔE at temperature T, then the diffusion coefficient is proportional to $\exp(-\Delta E/k_{\mathrm{B}}T)$. As the probability (Ω) of material movement from one site to another will depend on the activation energy due to the curvature difference, the probability of material movement is $\exp(-\Delta\gamma/T_1)$, where T_1 is a factor which is proportional to the temperature T. Depending on the above probability, the mass transfer takes place during sintering, i.e., the height of the point $P(x, y)$ is modified to $h(x, y) + \Omega \times (\Delta h/2)$ and that for $P'(x', y')$ is modified to $h'(x', y') + \Omega \times (\Delta h/2)$. The average width $(W = [\sqrt{\sum [h(x, y) - \bar{h}]^2/(N^2)}]$, where $\bar{h}$ is the average height and $N \times N$ is the system size) of the surface is calculated at each iteration. The value of W starts decreasing sharply initially and decreases slowly after a reasonably large time step when the surface is nearly equilibrated at a particular temperature. The long time width (W) of the surface is noted for various T_1 values. The equilibrated surface has been registered. The spectral densities $(S(k), k$ in Fourier space) of the surfaces at various T_1 values are calculated. The modifications in the fractal nature of the initial surface are noted by plotting $\log(S(k))$ versus $\log(k)$ for different values of k. If fractal correlation exists in the structure, the curve $\log(S(k))$ versus $\log(k)$ can be fitted to a straight line and the slope of that line, the fractal dimension, can be estimated [31] from the slope. Here it should be mentioned that in reality mass transfer from one site to another distant site could occur via the nearest neighbours only. However, in the simulation process this corresponds to a huge number of Monte Carlo steps vis-à-vis an enormously large computation time. However, as we are currently interested only in the effect of sintering temperature for large sintering time, the mass transfer from one source site to another distant target site, not a nearest neighbour site, was also allowed, keeping the number of Monte Carlo steps constant for all temperatures. In fact, this corresponds to the sintering phenomenon at various temperatures for a particular sintering time. It is worth mentioning that Fereydoon Family *et al* have shown that the final simulation results for the random filling model with surface diffusion in a square lattice are independent of whether the transport is to nearest sites or to sites that are not nearest neighbour sites.

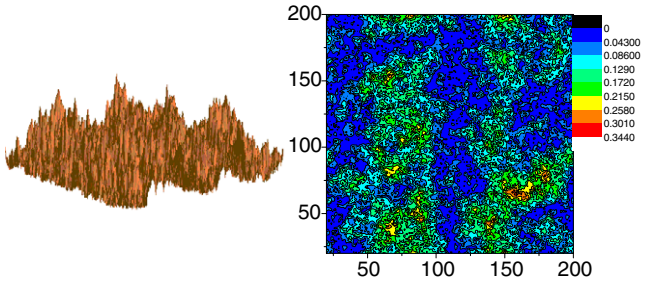

Figure 3. The initial self-affine fractal surface simulated using the spectral synthesis method for a fractal dimension 2.6.

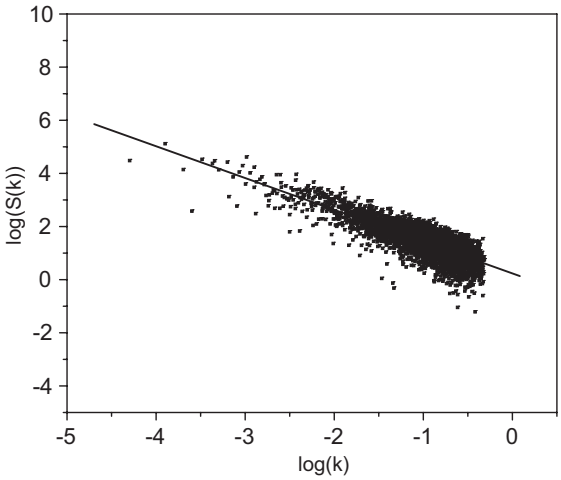

Figure 4. $\log(S(k))$ versus $\log(k)$ for the initial fractal surface with fractal dimension 2.6.

On the basis of the Fourier filtering spectral analysis method, an initial self-affine surface (200 × 200 system size) having a fractal dimension of 2.6 has been generated and is shown in figure 3.

The left part of figure 3 shows the surface (as a surface plot) and the right part shows the contour of the same surface. The verification of the fractal nature (with fractal dimension 2.6) is done by calculating the linear form of the $\log(S(k))$ versus $\log(k)$ curve as shown in figure 4. At this point, it should be mentioned that the spectral density $(S(k))$ for self-similar objects exactly follows a power law, i.e., an exact straight line behaviour in a $\log(S(k))$ versus $\log(k)$ plot. However, for a self-affine surface $\log(S(k))$ versus $\log(k)$

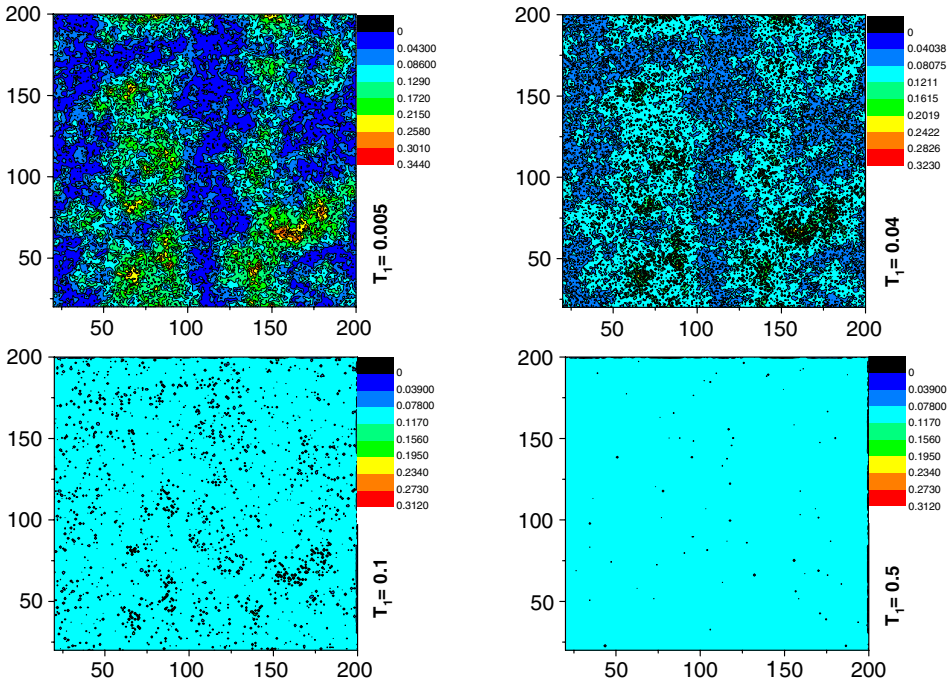

Figure 5. The surfaces for increasing T_1 values are depicted. It is evident that the surface becomes smoother with an increase in T_1.

follows a straight line behaviour but with statistical fluctuations around the line. However, the fluctuations increase more and more as the surface deviates from self-affine nature towards a non-fractal surface.

The contours of the surface at various T_1 ($T_1 \propto$ temperature) values are plotted in figure 5. It is evident from the figure that the surface roughness is reduced gradually as T_1 is increased and at high enough temperature the surface roughness is almost absent.

The variation of the surface width (W) and the calculated fractal dimension of the sintered surface with varying T_1 values are plotted in figure 6. It is seen that the value of W decreases gradually with temperature. The fractal dimension decreases more sharply than the width.

Figure 7 shows the spectral density plots of the surface at different T_1 values. It is seen that as the temperature is increased the fluctuations in $\log(S(k))$ versus $\log(k)$ are also increased indicating more and more deviation from self-affinity and also the absence of fractal correlation on the surface.

The corresponding fractal dimension (d_s), calculated from the slope of the $\log(S(k))$ versus $\log(k)$ plots, is plotted also in figure 6. It is seen that the value of d_s decreases from 2.6 to a value of 2.0 (representing a smooth surface) with increase in the temperature. As the fluctuation in the $\log(s(k))$ versus $\log(k)$ plot increases with increase in the value of T_1, the error bars are shown for the estimated fractal dimension.

The simulated fractal dimension and the experimentally observed fractal dimension are compared in figure 8 on a dimensionless reduced temperature (T/T_{initial}) scale. It is observed that in both cases the fractal dimension starts decreasing from the initial value of 2.6 and reaches the Euclidean dimension for the surface, i.e., 2.0. However, it is

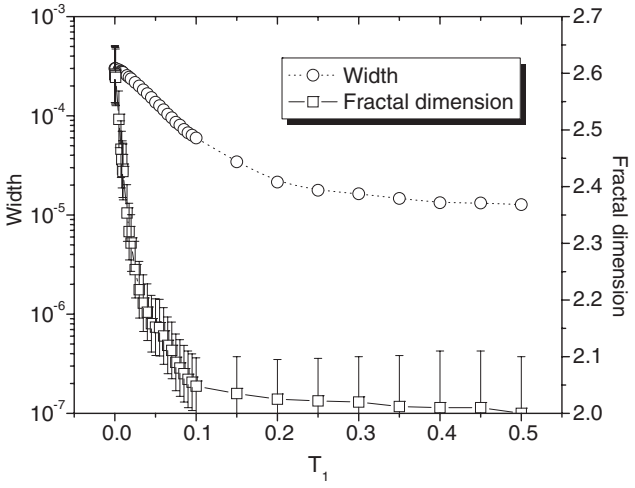

Figure 6. The reduction of the surface width and the decrease of the fractal dimension with an increase in T_1 are depicted. The initial fractal dimension of 2.6 reaches the value of ∼2.0 at a high enough value of T_1.

also observed that the fractal dimension is reduced somewhat more sharply in the case of experiment compared to that for the simulation. This has been attributed to the following two points:

(i) For the present samples, the grains are on the nanometric scale. As the available specific surface area is more than for the bulk grains, the rate of diffusion is expected to be somewhat faster, which leads to faster sintering vis-à-vis faster reduction in the fractal dimension.

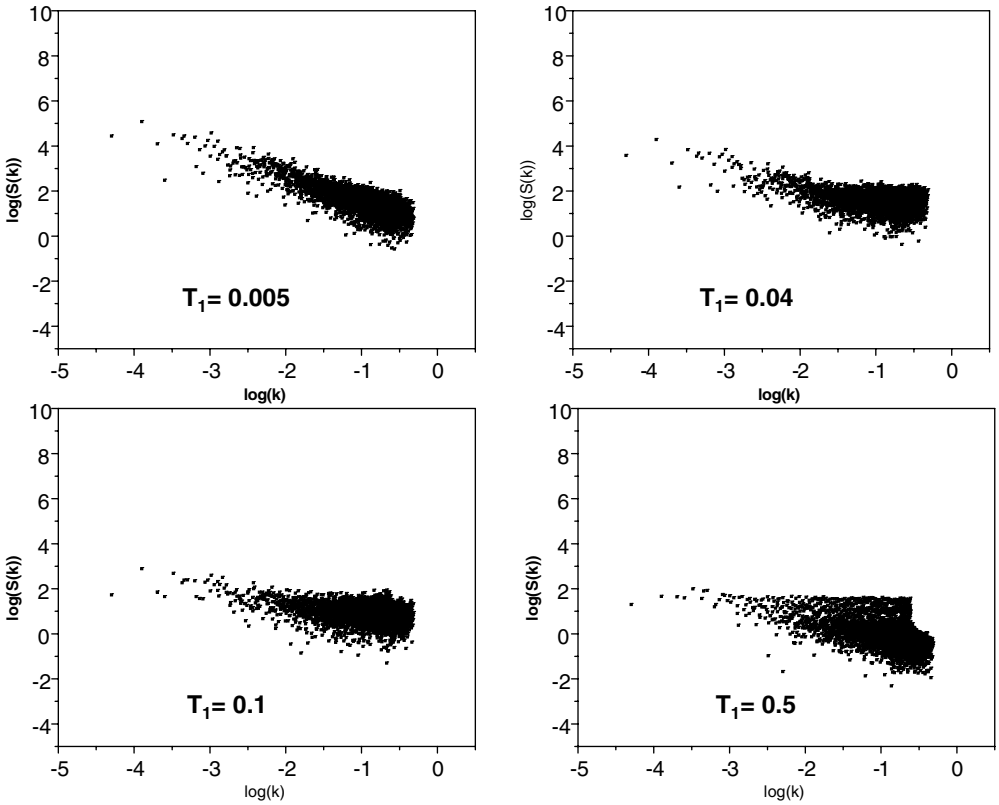

Figure 7. The spectral density of the evolving surface during sintering.

(ii) At relatively high sintering temperature there is always a finite and significant probability of mass diffusion in addition to the surface diffusion. The combination of diffusion processes results in an increase of the effective sintering rate. However, as the consideration of the mass transport (in three dimensions) in the whole grains makes the computation much more complex and also enormously time-consuming, for the present paper we restricted consideration to just the surface diffusion.

At this juncture, it is pertinent to discuss the nature of the transition of the fractal dimensionality that takes place during the sintering simulation. Normally, for a non-equilibrium system, in particular for pattern formation in growth processes, the transition in the pattern may either be gradual or be associated with some dynamical phase transition [32]. For example, in the case of fluid invasion in porous media [32–34], a dynamical phase transition associated with changes in local growth modes in a model porous medium has been predicted [32] by Cieplak *et al*. In this study it has been shown that below a critical contact angle, between the fluid and the pore interface, the fluid advancement pattern is smooth, while above the critical contact angle the pattern corresponds to a fractal one. In such a case, the local growth mode is governed by different instabilities and corresponding growth mechanisms, like 'burst', 'touch' and 'overlap' between neighbouring interfaces. However, in our present simulation it is observed that the transition in the fractal dimensionality remains gradual with respect to the time at a particular sintering

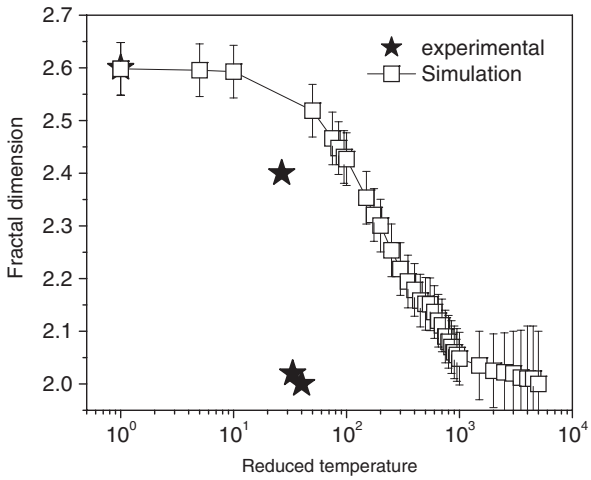

Figure 8. Variation of the fractal dimension with reduced sintering temperature.

temperature. The occurrence of such a gradual transition, vis-à-vis the absence of a dynamical phase transition of the fractal dimensionality, may be attributed as due to the nature of mass transport from one site to another solely via diffusion throughout the sintering process.

5. Conclusions

A USAXS study revealed that the fractal correlation for the rough surfaces of non-sintered grains of Nd_2O_3 doped CeO_2

is diminished under sintering. A relatively high surface fractal dimension (∼2.6) in the non-sintered ceramic gradually reduces to the normal Euclidean surface dimension of 2.0 at high enough sintering temperature. The Monte Carlo based computer simulation established that such smoothing of fractal rough surfaces under sintering is possible due to the diffusion transport of materials from regions of higher curvature to regions of lower curvature. As the fractally rough surface, being in a metastable state, 'tries' to minimize its surface energy during sintering, a smooth surface is gradually developed with increase in the sintering temperature. The reduction in the roughness from the USAXS experiment follows a relatively sharp trend compared to that for the simulation. This difference has been attributed as due to the faster sintering in nanoceramics due to the availability of larger specific surface area as compared to the bulk case and also due to the additional mass diffusion transport mechanism over and above the surface diffusion mechanism. Although the present simulation deals only with surface diffusion based mass transport, in the next step in the near future, consideration of the mass diffusion in a three-dimensional network, in addition to the surface diffusion, will be attempted within the computational limitations. In addition, more experimental investigations on the effect of sintering temperature and time on the various fractal systems are called for.

Acknowledgments

The authors would like to thank Dr O Spalla and Dr A Thill of LIONS, CEA, Saclay, France, for providing access to the LIONS USAXS facility.

References

[1] Mandelbrot B B 1982 *The Fractal Geometry of Nature* (New York: Freeman)
Mandelbrot B B 1977 *Fractals, Form and Dimension* (San Francisco, CA: Freeman)
[2] Sen D, Mazumder S and Tarafdar S 2002 *Appl. Phys.* A **74** S1049–51
[3] Radlinski A P, Radlinska E Z, Agamalian M, Wignall G D, Linder P and Randl O G 1999 *Phys. Rev. Lett.* **82** 3078
[4] Sen D, Mazumder S, Chitra R and Chandrasekaran K S 2001 *J. Mater. Sci.* **36** 909
[5] Bale H D and Schmidt P W 1984 *Phys. Rev. Lett.* **53** 596
[6] Mazumder S, Sen D, Patra A K, Khadilkar S A, Cursetji R M, Loidl R, Baron M and Rauch H 2004 *Phys. Rev. Lett.* **93** 255704
[7] Mazumder S, Sen D, Patra A K, Khadilkar S A, Cursetji R M, Loidl R, Baron M and Rauch H 2005 *Phys. Rev.* B **72** 224208
[8] Schimidt P W 1991 *J. Appl. Crystallogr.* **24** 414
[9] Kingery W D, Bowden H K and Uhlmann D R 1976 *Introduction to Ceramics* (*Wiley Series on the Science and Technology of the Materials*) 2nd edn (New York: Wiley) p 1032
[10] Glatter O and Kratky O 1982 *Small Angle X-Ray Scattering* (London: Academic) pp 329–58
[11] Guinier A, Fournet G, Walker B C and Yudowith L K 1955 *Small Angle Scattering of X-Rays* (New York: Wiley) pp 167–95
[12] Texeira J 1988 *J. Appl. Crystallogr.* **21** 781–5
[13] Maki Y, Matsuda M and Kudo T 1971 *US Patent Specification* 3,607,424
[14] Bedekar V and Tyagi A K 2007 *J. Nanosci. Nanotechnol.* **7** 1–7
[15] Cho Yong S, Glicksman H D and Amarakoon V R W 2004 *Encyclopedia of Nanoscience and Nanotechnology* vol 1, ed H S Nalwa (California: American Scientific Publishers) p 727
[16] Logothetis E M 1976 *National Symposium on Ceramics on the Service of Men* (Washington, DC)
[17] Bonse U and Hart M 1965 *Appl. Phys. Lett.* **7** 238–40
Bonse U and Hart M 1966 *Z. Phys.* **189** 151–62
[18] Lambard J, Lesieur P and Zemb T 1992 *J. Phys.* I **2** 1191–213
[19] Lake J A 1967 *Acta Crystallogr.* **23** 191–4
[20] Mazumder S, Sen D, Sastry P U M, Chitra R, Sequeira A and Chandrasekaran K S 1998 *J. Phys.: Condens. Matter* **10** 9969–74
[21] Freltoft T, Kjems J K and Sinha S K 1986 *Phys. Rev.* B **33** 269
[22] Allouche J P and Shallit J 2003 *Automatic Sequences: Theory, Applications, Generalization* (Cambridge: Cambridge University Press)
[23] Mildner D F R and Hall P L 1986 *J. Phys. D: Appl. Phys.* **19** 1535
[24] Bhatia S R 2005 *Curr. Opin. Colloid Interface Sci.* **9** 404–11
[25] Shah S A, Chen Y L, Ramakrishnan S, Schweizer K S and Zukoski C F 2003 *J. Phys.: Condens. Matter* **15** 4751–78
[26] Mon K K 1986 *Phys. Rev. Lett.* **57** 866–8
[27] Family F 1986 *J. Phys. A: Math. Gen.* **19** L441–6
[28] Aharonov E and Rothman D 1996 *J. Geophys. Res.* **101** 2973–87
[29] Sen D, Mazumder S and Tarafdar S 2002 *J. Mater. Sci.* **37** 941–7
[30] Schmid H-J, Al-Zaitone B, Artelt C and Peukert W 2006 *Chem. Eng. Sci.* **61** 293–305
[31] Saupe D 1988 Random fractals algorithms *The Science of Fractal Images* ed H O Peitgen and D Saupe (New York: Springer) pp 71–136
[32] Cieplak M 1988 *Phys. Rev. Lett.* **16** 2042–5
[33] Martys N, Robbins M O and Cieplak M 1991 *Phys. Rev.* B **44** 12294–305
[34] Martys N, Cieplak M and Robbins M O 1991 *Phys. Rev. Lett.* **66** 1058–61